The new Hydro-mechanical Solar Tracker: Performance Testing with a PV Panel

Kant E. Kanyarusoke, and Jasson Gryzagoridis

Abstract— This paper describes work carried out to test the performance of a newly invented solar tracker. It is a gravity driven, bladder-flow controlled, Hooke coupled inclined non polar axis solar tracker. The performance of the tracker when coupled with a PV panel was first modelled in MATLAB® using the Perez anisotropic diffuse radiation and the King cell temperature models. Experiments with two identical 90 Wp panels were done over a 40 day period in outdoor conditions. One PV panel was fixed on optimised slope, the other, was driven by the tracker about a similarly sloped axis. Weather data consisting of total and diffuse radiation, ambient temperature and wind speed was also collected using a Campbell Scientific weather station adjacent the panels. This data was used to simulate performances of the panels in the MATLAB® model. TRNSYS simulations were also done for the two panels. The three sets of results were compared. It was found that the tracked panel yielded 34% more energy than the fixed one and that the experimental results correlated more closely with the MATLAB® models than with TRNSYS ones. Results also indicated that the efficacy of the tracking device could be influenced by the timing of cloudiness during the day and by wind speed.

***Index Terms*— MATLAB, PV panel, Single axis tracker, Solar energy, Solar Tracking, TRNSYS.**

1 INTRODUCTION

Previous work in [1] indicated that most of the existing solar tracking devices were either unsuitable or unavailable for domestic home use in sub-Sahara Africa. Therefore, a new device, designed with the region's conditions of low skill base, bi-hemispherical tropical location and low disposable incomes in mind, was invented by the authors. It is described in a patent application by Cape Peninsula University of Technology (CPUT) [2]. A line sketch of the tracker is shown in Fig.1. Its photograph is given later in the experimental section of this paper.

Work by other inventors and researchers (e.g. [3] – [7]) shows that energy gains between 15 and 49% are possible when using different trackers, depending on whether the tracking is on single or on double axis The work in this paper aimed to find out how much electrical energy gain could be obtained from using the invented device at the Bellville campus of CPUT – coordinates: 33.935°S, 18.644°E, 68.5 m. In addition, we wanted to know how predictions by TRNSYS simulation and by a MATLAB® based code using actual weather data, compared to actual energy yields.

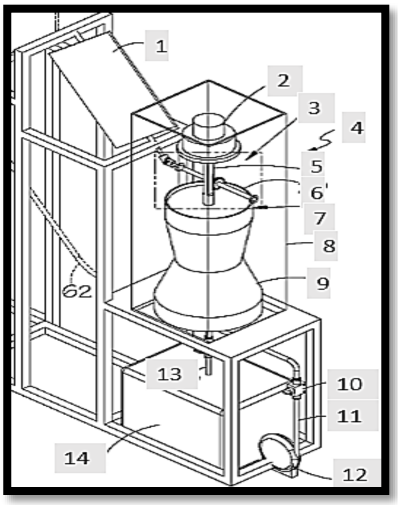

Fig. 1. The prototype solar tracker

1- PV panel 2 - Drive weight 3 - Gear rack assembly 4- Tracker assembly 5 - Rack 6 - Gear shaft 7- Piston 8 - Mechanism housing 9 – Bladder 10 - One way valve 11 - Bladder feed pipe 12 – Pump 13 - Solenoid valve 14 Water tank

2 THEORETICAL MODELLING

In this section, the incident energy on an inclined photovoltaic (PV) panel – which is described by Duffie and Beckman [8] is summarised first. The panel's parameters at the manufacturer test conditions are also deduced. A method for analytically determining electrical energy yield from the PV panels is given.

2.1 Incident energy on an inclined panel

Fig. 2 illustrates the important angles and incident energy terms on a southern hemisphere panel sloped at angle $\beta°$ and with azimuth $\psi°$**.** Beam and circumsolar radiation reach the panel at a variable angle of incidence $\boldsymbol{i°}$**.** At this instant, the sun is viewed at an azimuth angle $\psi_s°$, and either an elevation $\alpha°$ or a zenith angle $z°$. Perez *et al.* [9] give an expression for total incident radiation on the panel $\boldsymbol{G_{panel}}$ as in equation (1) – with terms defined as in equations (2-4) [8].

$$G_{panel} = G_{bh}R_b + G_d(1-F_1)\left(\frac{1+\cos(\beta)°}{2}\right) + G_dF_1\frac{a}{b} + G_dF_2\sin(\beta°) + G_h\rho_g\left(\frac{1-\cos(\beta°)}{2}\right) \quad (1)$$

$$R_b = \frac{G_{bpanel}}{G_{bh}} = \cos(i°)\sec(z°) \quad (2)$$

. This work was supported in part by the Cape Peninsula University of Technology Research Fund, Grant RK/23.

K. E. Kanyarusoke, Cape Peninsula University of Technology, P O Box 1906, Bellville Cape Town (7535), South Africa (e-mail: kanyarusokek@cput.ac.za).

J. Gryzagoridis, Cape Peninsula University of Technology, P O Box 1906, Bellville Cape Town (7535), South Africa (e-mail: gryzagoridisj@cput.ac.za).

Where: G_h is total radiation on a horizontal surface – consisting of the beam/circumsolar part, G_{bh} and the diffuse part; G_d. Ground reflectivity is denoted as ρ_g. F_1 and F_2 are empirical circumsolar and horizon brightness functions of z and sky brightness determined according to the Perez model instructions [9]. Parameters a, and b are given by equations 3 and 4 respectively [8].

$$a = \max(0, \cos(i°))\ ;\ b = \max(\cos(85°), \cos(z°)) \quad (3, 4)$$

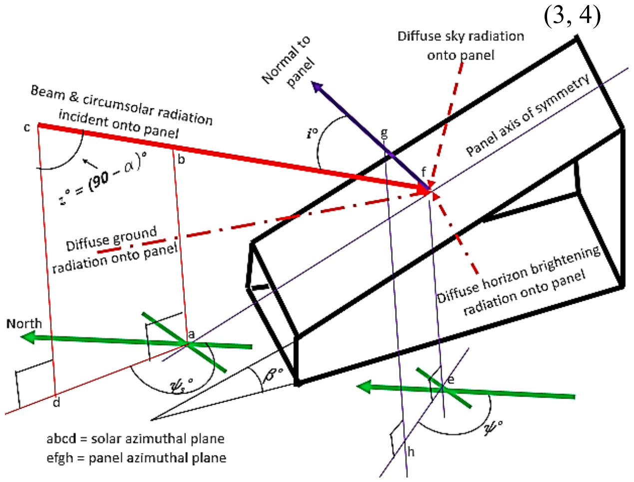

Fig. 2. Important angles and incident energy components onto an inclined panel

For a given panel slope β and azimuth ψ, the angles i, $\psi_s°$ and z (or α) depend on latitude $L°$, day of year n, and time from solar noon, t. Expressions for these are available in standard solar energy engineering text books such as [8], [10] and [11].

When either the panel's slope or azimuth is made to vary (as in many solar tracking systems), vector algebra can be used to determine the new direction of the surface's normal, and hence, the angle of incidence. In the experiments of section 4 for example, one of the panels tracks about a fixed axis (β_{axis} = 30°). In that case if the panel rotates an angle $\phi°$ from a start position of β = 90°, ψ = 270° (i.e. facing East), the algebra gives its slope and azimuth as in equations (5) and (6) respectively.

$$\beta = \cos^{-1}(\cos\beta_{axis}\sin\phi) \quad (5)$$

Before Solar noon:

$$\psi = 180 + \cos^{-1}\sqrt{1 - \frac{1}{1 + \tan^2\phi\sin^2\beta_{axis}}} \quad (6a)$$

After solar noon:

$$\psi = 180 - \cos^{-1}\sqrt{1 - \frac{1}{1 + \tan^2\phi\sin^2\beta_{axis}}} \quad (6b)$$

2.2 The PV panel and its characteristics

Although [8] uses a 5 parameter model for PV panels, TRNSYS simulation recommends a 4 parameter (I_L, I_0, R & n) model for mono-crystalline silicon cells [12]. Since the work here aimed to compare results with TRNSYS predictions, the latter model was used in the MATLAB® formulation. The characteristic equation relating current I to voltage V is then given as:

$$I = I_L - I_0\left[\exp\left(q(V+IR)/nkT_cN_s\right) - 1\right] \approx I_L - I_0\left[\exp\left(q(V+IR)/nkT_cN_s\right)\right] \quad (7)$$

Where: q is the electron charge, 1.602E-19 C and k is Boltzmann's constant, 1.381E-23 J/K. For the panels used, N_s = 36 cells.

Fig. 3 is a graphical representation of the equation – and it shows how to geometrically locate the operating point for maximum power generation ($d(IV)$ = 0) using a straight edge. The slope of the edge is varied until its tangency to the characteristic curve is exactly half way between edge intercepts on the two axes.

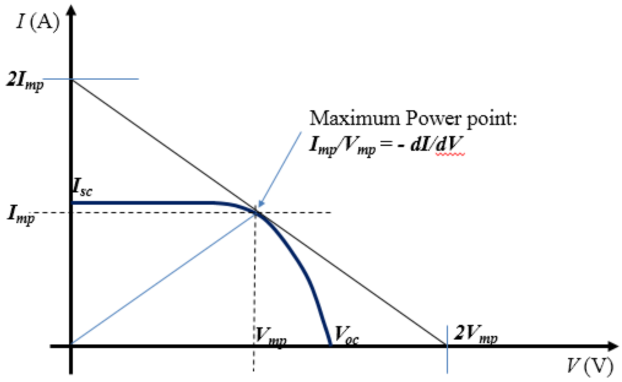

Fig. 3. The 4-parameter model characteristic for a PV panel

Manufacturer panel specifications give short circuit current I_{sc}, open circuit voltage V_{oc}, maximum power current and voltage I_{mp} and V_{mp} based on standard conditions of G_{std} = 1000 W/m²; $T_{ambient}$ = 25°C = 298.15 K; v_{wind} = 1 m/s; and optical air mass m_{air} = 1.5 at sea level. The four parameters at those conditions ($I_{L\text{-}std}$, $I_{0\text{-}std}$, R and n) can be determined by solving the given 3 instances of equation (7) and its differential at maximum power using suitable software. In the present case, the standard parameters were computed using a MATLAB® script and are given in Table I.

Table I. The test panels: key specifications and standard test parameters

Manufacturer's specifications	Standard conditions parameters
I_{sc} = 5.50 A	$I_{L\text{-}std}$ = 5.5 A
V_{oc} = 22.4 V	$I_{0\text{-}std}$ = 1.721E-10 A
I_{mp} = 4.90 A	R = 0.1001 Ω
V_{mp} = 18.4 V	n = 1.001
α_{isc} = +1.55 mA/K	G_{std} = 1000 W/m² (given)
α_{voc} = -79.2 mV/K	NOCT = 45°C = 318.15 K (given)
α_W = - 0.46%/K	

2.2.1 *Operating conditions characteristics*

Operating conditions differ from those during tests – and therefore parameter values in Table I do not reflect actuals in practice except for the 'ideality' factor n and the internal module resistance R. In earlier work [13], equations (8) to (10) from [8] and [14] were used to relate panel currents to incident radiation and module cell temperatures. The same equations are applicable here.

$$I_L = \frac{G_{panel}}{G_{std}}\left[I_{L-std} + \alpha_{isc}(T_c - 298.15)\right] \quad (8)$$

$$I_0 = I_{0-std}\left(\frac{T_c}{298.15}\right)^3 \exp\left(47.04822 - \frac{14027.427}{T_c}\right) \tag{9}$$

$$T_c = T_{back} + \frac{G_{panel}}{G_{std}}\Delta T \tag{10a}$$

$$T_{back} = T_a + G_{panel}\exp(a' + b' v_w) \tag{10b}$$

Where $\boldsymbol{T_{back}}$ and $\boldsymbol{T_a}$ are panel backside and ambient temperatures; $\boldsymbol{a'}$, $\boldsymbol{b'}$ and $\boldsymbol{\Delta T}$ are respectively -3.56, -0.075 and +3 for a glass-cell-polymer sheet open rack mounting used in the experiments below.

Equations (8) – (10) are used along with the fixed values of $\boldsymbol{R}$ and $\boldsymbol{n}$ in Table I to determine the characteristics of the panel at any given instant.

2.2.2 *Energy yield from a PV panel*

Parameters in equation (1) were evaluated for the recorded actual values of $\boldsymbol{G_h}$ and $\boldsymbol{G_d}$ in MATLAB®. Hence, $\boldsymbol{G_{panel}}$ was computed for each instant. Consequently, all terms in the characteristic curve equation (7) could be determined. In the experiments below, Maximum Power Point Trackers (MPPTs) were used – and therefore, instantaneous power generated could be computed by locating the point of maximum power in Figure 3 – as represented by the approximation in equation (11).

$$\frac{dI}{dV} + \frac{I}{V} = 0 \approx \frac{\delta I}{\delta V} + \frac{I}{V} \tag{11}$$

Incremental values of 0.01$\boldsymbol{I_L}$ for $\boldsymbol{I}$ between 0.30$\boldsymbol{I_L}$ and 0.98$\boldsymbol{I_L}$ in MATLAB® were used to check satsfaction of this condition, and hence, to determine the maximum power point, ($\boldsymbol{I_{mp}}$,$\boldsymbol{V_{mp}}$). By recording these $\boldsymbol{I_{mp}}$ and $\boldsymbol{V_{mp}}$ values across each day during the period of interest, the maximum possible total electrical energy yield from the panels was determined by numerical integration.

3 TRNSYS MODELLING

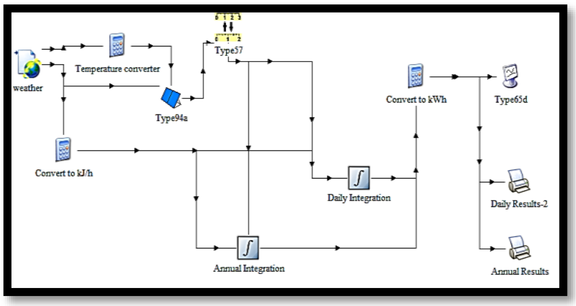

Fig. 4. The TRNSYS model for determining PV energy yield.

In Fig. 4, the type 94a PV panel was configured for both fixed and single inclined axis tracking to get two sets of results.

4 EXPERIMENTAL INVESTIGATIONS

4.1 Tools and Equipment

- 1 - Prototype gravity driven, bladder flow controlled hydro-mechanism adopted for solar tracking.
- 2 – Mono crystalline silicon Solar panels: as specified in Table I. Manufacturer: SetSolar, Cape Town.
- 2 – MPPT charge controllers 10 A from SetSolar.
- 2 – Batteries: Deep cycle lead-acid; 12 V; 105 Ah.
- 2 – Bulbs MR-16 dichroic halogen lamp; 50 W, 3000 hours.
- Weather station – Campbell Scientific. Consisting of: 1 Kipp Zonen CMP06 Pyranometer, ISO First class; 2 SP LITE silicon Pyranometers (with one shaded to measure diffuse radiation), a 03101 R.M Young anemometer and an ambient dry bulb temperature probe.
- 1 - 32 channel Campbell Scientific measurement and control data logger.
- Three weather proof enclosures: two for the batteries and charge controllers, the other for the electric bulbs.

4.2 Set up and Procedure

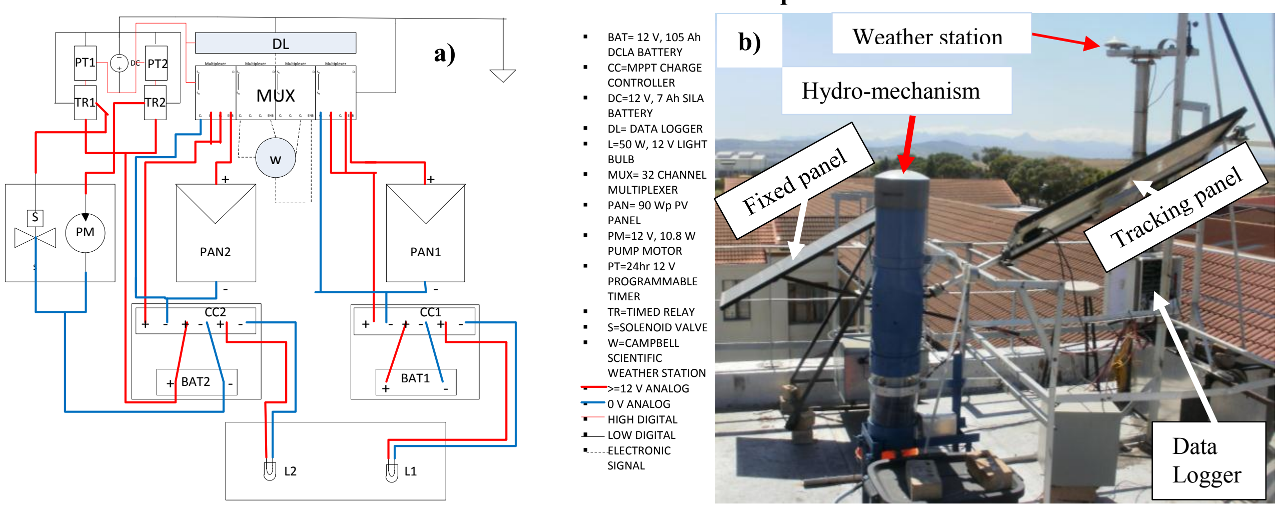

Fig. 5. Experimental set-up: a) wiring diagram b) Actual layout

- One 90 Wp solar panel was set up facing true north, sloped at 30° from the horizontal (the TRNSYS derived optimal slope for the site). The mount for the panel had been designed with an adjustable mechanism to vary the angle – which was measured using a smart phone with a protractor application installed - and crosschecked by trigonometric computations. Parallel to this, but offset southward, a stand for the tracking panel and tracking mechanism was erected. The southward offset was to ensure that the tracking PV panel did not shade the fixed one during operation.

- A shaft inclined at 30°, supported on the stand with self-aligning ball bearings, was connected to the new tracker's Hooke coupling. The PV panel was centrally attached to this shaft using suitably designed brackets. A counter weight was centrally attached to the shaft on the backside of the PV panel, thus ensuring stability.
- The panels, batteries, charge controllers, bulbs, data logger and the tracking mechanism were wired up as in Fig. 5. The system was run for the planned 40 day period: 15 Nov – 24 Dec 2015. Occasionally during the period, readings of panels' voltage and current were taken manually using a hand held voltmeter and clamp ammeter. This was only meant to randomly cross check with the automatically recorded 15 minute data in the logger. The bulbs were left on during the entire period to ensure the batteries always started in a minimum charge condition – thus causing the panels to generate maximum power during the day.
- Weather data: i.e. horizontal surface total irradiance, G_h (W/m^2), diffuse irradiance G_d (W/m^2), ambient temperature, T_a (°C) and wind speed v_w (m/s) were recorded in the logger. The data acquisition and processing circuitry had been configured to sample every 2 s, totalise the data, and store the average values over each 15 minute interval.
- Similarly, interval average voltages and currents from both panels were recorded in the logger at 15 minute intervals.

4.3 Analysis

The analysis involved two approaches: one was the use of the raw weather data in the models to derive or predict the performance for each of the panels. The other approach was the extraction of actual measured power in order to deduce daily electrical energy output which could be compared with predictions from TRNSYS simulations and from the MATLAB® model.

4.3.1 Using Weather data

Solar radiation data from the logger was reconfigured in two MATLAB® scripts using equations (1) – (6) to derive 15 minute incident solar power on each panel, $W_{inc\text{-}panel}$. The ground reflectivity ρ_g (roof and faroff ground objects) was assumed to be 0.2. Data for ambient temperature and wind speed were used in the second part of the scripts to determine panel cell temperatures, T_c in accordance with equations (10). Then, equations (8), (9) and (11) were programmed to give the maximum power point, and hence, the peak power generation every 15 minutes for each panel, $W_{out\text{-}panel}$. The third part of the scripts totalised (i.e. integrated power), compared daily output energy with input incident energy and graphed the panels' performances.

4.3.2 Using Measured Voltage and Current data

Daily electrical energy production from each panel was found by numerical integration of the power data. The trapezium approximation was used because of its simplicity. In total, there were up to 62 time intervals in a day ranging from 5 am to 8 30 pm. The energy data was transferred to MS EXCEL spreadsheets for comparison with the outputs from the TRNSYS simulation and the MATLAB® model.

4.4 Results

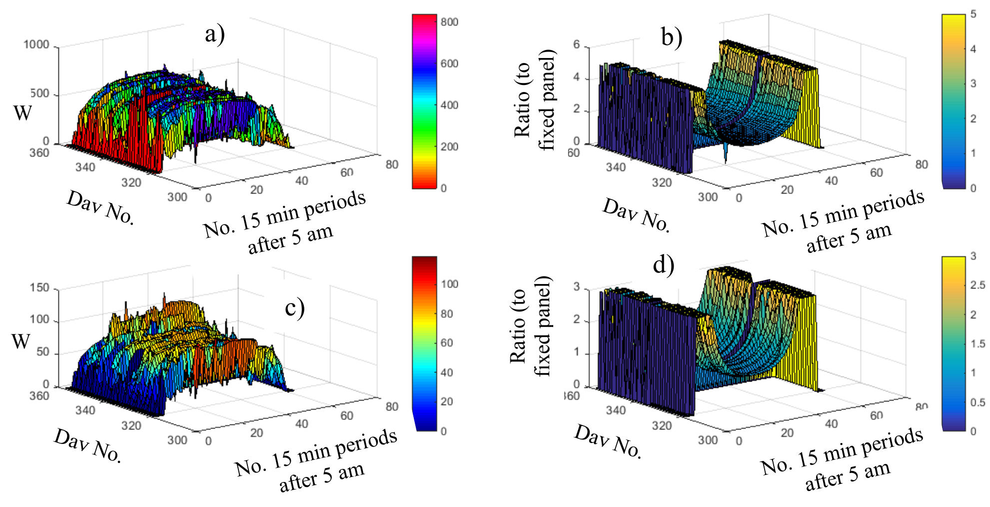

Fig. 6. Summary of experimental data for period: 15 Nov-24 Dec 2015: a) Incident solar radiation power on solar tracking panel; b) Ratio of incident power on tracking to that on non tracking panel; c) Measured electrical power output of the solar tracking panel d) Ratio of measured power from tracking to that from the non-tracking panel.

Of the targeted 40 days, there were full data for 39 days. Data for day no. 339 (5th Dec 2015) was incomplete because the data logger battery had to be recharged for most part of the day. Data for this day is therefore excluded from the report.

4.4.1 Overview

Fig. 6 gives a graphical overview of the results. In a) the quarter hourly incident power on the tracking panel as computed in section 4.3.1 is depicted. Rather than present a similar one for the non-tracking panel, Fig. b) gives the ratio between the two amounts of incident power. It was found that very early morning and late evening, the ratios were very high - due to the Perez horizon brightening effect in equation (1). Hence, to get a scalable figure, the depicted ratios at these times were capped to 5 although actual values were left intact in the primary data for other computations. Fig. 6c) gives the tracking panel's actual computed output power from section 4.3.2. Fig. 6d) gives the output power gain ratio computed from actual measurements. Like in b), it is capped, but this time at 3.

4.4.2 Observations during experiments

During the course of experiments, three phenomena were observed: effect of windy conditions; effect of clouds/rain; and propensity of fixed panel to get dirty/dusty (and difficulty to clean it) relative to the tracking one.

Windy conditions stronger than gentle breezes ($v_w \geq 3.5$ m/s) tended to affect the tracking mechanism through reduction of panel rotary speed between intended start-stop positions. This led to tracking errors, especially in mid-morning hours – since the travel time was fixed.

Power and energy computations at the end of each day showed that clouds and rain tended to affect the day's tracking energy gain ratio depending on which times of the day were cloudy/rainy – with late mornings and early afternoons being less consequential than mid-mornings and late afternoons.

Besides a tendency for dust to settle and remain on the fixed panel, it was noticed that birds preferred its upper edge to that of the tracking panel as a resting place (or was it for surveillance purposes?). Consequently, in addition to dust, bird droppings were more common on the fixed panel, making it more involving to clean and maintain.

The overall effects of the first two observations led to a qualitative two dimensional performance possibility space depending on tracking accuracy (low average wind speeds) and extent of beam radiation (i.e. absence of cloudiness) during the day. The descriptive statistics for the 39 days were consequently reconfigured in 4 performance quadrants as in Table II. Performances on typical days in each quadrant are illustrated in Fig. 7.

Table II. Descriptive statistics of tracking panel performances

Quadrant Number	Description	Number of days
1	*Clear sky:* $v_w < 3.5$	11
2	*Clear sky;* $v_w \geq 3.5$	11
3	*Cloudy:* $v_w \geq 3.5$	9
4	*Cloudy;* $v_w < 3.5$	8

4.4.3 Comparison of performances

Fig. 8 gives the comparative performances of fixed and tracking panels. In meeting the other objectives of this work, it compares actual energy yield with each of the models' predictions.

5 RESULTS DISCUSSION

In this section the results arrived at during this work are interpreted and explained. Where appropriate, implications on possible applications of the tracking mechanism are deduced.

5.1 General observations (Fig. 6)

5.1.1 Incident radiation

The tracking panel generally received more radiation on it in spite of fluctuations throughout the day. For the entire period, the incident energy gain ratio was found to be 1.53. Whereas this seems to be a relatively high value, it is different from – and actually - does not necessarily reflect energy output ratios from devices run by the tracker – as evidenced by a 1.34 ratio for the latter in this case. Fig. 6b shows that, most relative gains were made in the hours between daybreak and about 9 am (240 min) and then much later in the day, between 5 pm and 7 pm (720-840 min). This is as expected because the difference in angles of incidence for the two panels is greatest at these times. The practical implication of this result is that the tracker would be most useful in systems seeking to extend solar energy harnessing to these times.

5.1.2 Output electrical energy

Electricity yield approximately followed the pattern of incident energy on each panel. There was limited energy gain from tracking between mid-mornings and early afternoons, with 20 of the 39 days indicating gain ratios of just below 1 in the solar noon hours (ranging between 450 and 540 min). Whereas theory indicates that the outputs in these hours should always be equal, giving a ratio of 1, random tracking errors occasioned by the open loop control design of the tracker [2] led to this variation. Even with these errors however, the overall electrical energy gain ratio for the period, remained relatively high at 1.34 - as pointed out above.

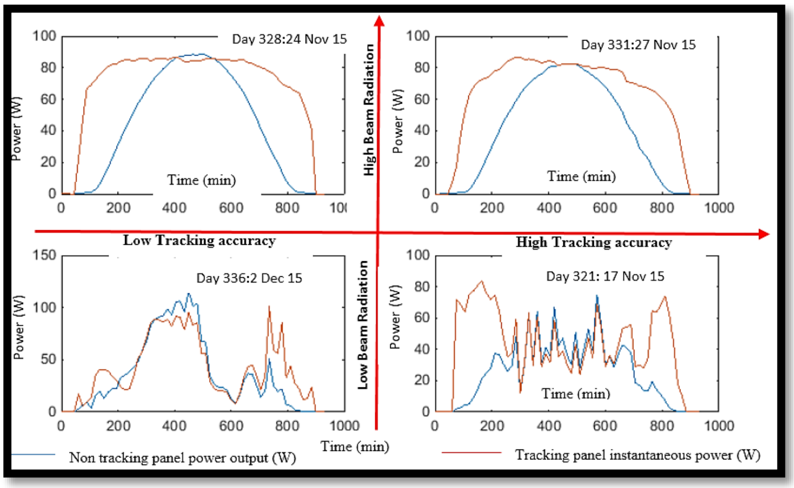

Fig. 7. Representative days in performance quadrants: 1st quadrant: High beam radiation with high tracking accuracy; 2nd quadrant: High beam radiation with some tracking errors; 3rd quadrant: Low beam radiation with tracking errors; 4th quadrant: Low beam radiation with high tracking accuracy.

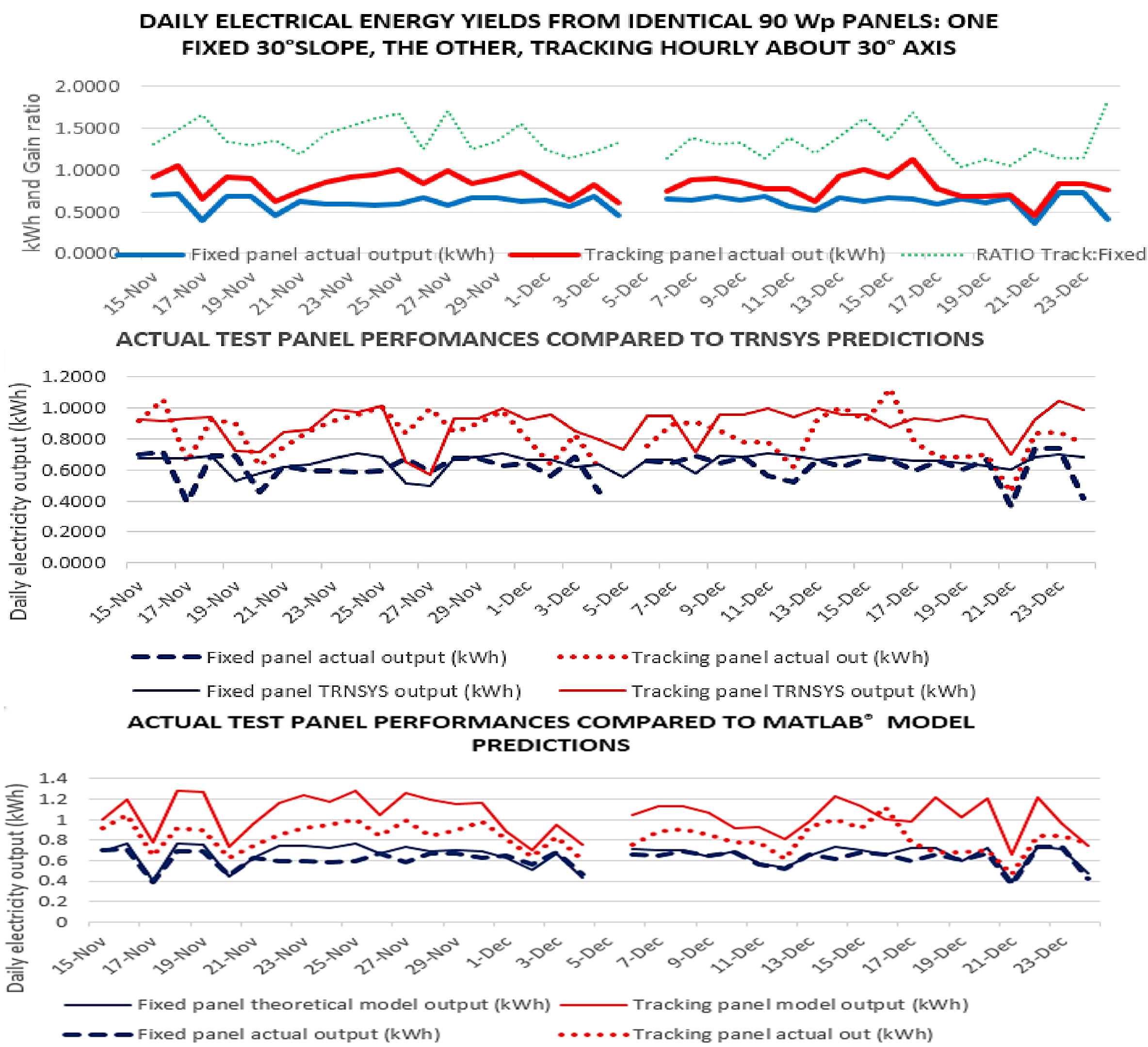

Fig. 8. Actual daily energy outputs compared with TRNSYS and MATLAB® predictions

5.1.3 Thermodynamic efficiencies of the panels

Efficiency is generally defined as a ratio of an output of what is desired to the total input in similar units of measure. For the fixed panel in the period, this simplifies to the ratio of output electrical energy to the incident solar energy on panel cells. It worked out as 16.7% (or 23.078

kWh/149.882 kWh). This was approximately in line with the manufacturer's claim of 17%. A similar ratio for the tracking panel was 14.66% (or 33.609 kWh/229.3 kWh). This latter value however, is not the exact efficiency of the tracking system. The system consumed electrical energy to operate it. Each of the electronics circuits for the pump and solenoid ran full time at 20 mA, 12 V from the data logger battery. The 5 W solenoid valve ran 12 times a day for 6 s each time. The 10.8 W pump ran once a day for 55s. This gave a total combined consumption of 0.0104 kWh from the battery being charged by the tracking panel. Consequently, the tracking system overall energy efficiency η_{track} was 14.62%.

It is seen that although the electrical energy output is increased significantly by the solar tracker, the energy efficiency is remarkably reduced. This could be explained from cell temperature considerations. Tracking increases photocell exposure to beam radiation which in turn increases both numbers of electron-hole pairs generated and their velocities. This increases average kinetic energy at the cell junctions, and hence, thermodynamic temperature T_c. Light current I_L increases from increased properly directed electron-hole pairs (thermodynamic work) but so does the reverse diode current I_o – from misdirected ones - at an even higher rate. The combined effect of these is to increase useful power while at the same time increasing the proportion of incident energy converted to thermal. Hence, the negative power coefficient (α_W) quoted by the manufacturer (see Table I).

5.2 Detailed performance (Fig. 7)

Table II shows that about half of the days were in the 2nd and 3rd quadrants of Fig. 7. The tracking accuracy therefore has room for improvement. This could be done either by adjusting the solenoid valve timing from 6 s or by adopting a closed loop control system. While the former affects overall gain ratios, the latter - for technical reasons - was considered inappropriate in the market for which the tracker is intended.

Perhaps the most important result in Fig. 7 is the one that shows effects of diffuse radiation on energy gain ratios. This is manifested in the 3rd and 4th performance quadrants – where there was a total of 17 days. The combined ratio in these quadrants was found to be 1.30 as opposed to 1.37 for the 22 days of high beam radiation in the 1st and 2nd. On its own, this result shows that clear skies - tend to favour tracking. But there is more: The daily gain ratios for the 17 days ranged between a minimum of 1.1247 on day 353 and a maximum of 1.6627 on day 321 (see Fig. 6 for the latter) - depending on times during the day when the sky was cloudy. If in mid mornings or late afternoons, the gain ratio was low. It was higher if cloudiness was experienced around late morning to early afternoon. The issue here is the unpredictability of when skies will be clear, and therefore, the stochastic nature of tracking reliability in such circumstances.

5.3 Modelling efficacy comparisons (Fig. 8)

To determine the efficacy of the model in section 2 and of TRNSYS simulation, bivariate correlation analyses were done on fixed and tracking panel electric output results using SPSS software. This yielded 6 Pearson correlation coefficients for the 3 possible combinations of: MATLAB®, TRNSYS and Experimental. The results are summarised in Table III.

Table III. Pearson correlation coefficients for daily electrical energy outputs using different methods: N = 39: significant at the 0.01 level, 2 tailed.

	EXPT.	TRNSYS	MATLAB	
EXPT.		0.546	0.718	FIXED PANEL
TRNSYS	0.525		0.648	
MATLAB	0.672	0.575		
	TRACKING PANEL			

These statistics together with the graphs of Fig. 8 show that while there was significant positive correlation for all pairs, the MATLAB® model agreed most closely with the experimental work on fixed panel results. The closer agreement than TRNSYS in both fixed and tracking could be attributed to the MATLAB® model's use of actual weather data – while TRNSYS uses historical statistical data. There was a slight drop in the MATLAB®'s model agreement with experimental results when it came to tracking (0.718 to 0.672). This could be attributed to tracking errors – since the model assumed exact 15° hourly tracking. In summary therefore, it could be said that where actual weather data is known with a high degree of certainty, the MATLAB® model would be the preferred analysis tool to estimate PV electrical energy yield when the latter are connected to operate at maximum power points. Short of actual weather data, however, TRNSYS would still remain a fairly reliable tool.

6 Conclusion

This paper has described testing of a newly invented - solar tracking device. The device powered a PV panel tracking about a non polar inclined axis. The axis slope corresponded to a TRNSYS optimised value for a fixed PV installation at the site. The testing was done against three reference settings: a real identical panel at the optimised fixed slope; a virtual identical panel, tracking the sun about an identical axis in TRNSYS simulation; and a virtual identical panel tracking the sun about the same axis, in exactly identical weather conditions but in a MATLAB® simulation environment.

During development of these tests, a simple graphical method to locate the maximum power point on the characteristic of a PV panel was explained. A MATLAB® script to deduce manufacturer standard characteristic parameters was written as a precursor to developing a new model that would use real time weather data to predict panel performance.

Experiments were done over a period of 40 days, registering 2457 valid sets of readings out of a possible total 2520 (i.e. 97.5%). Each set recorded: day, time, 4 pieces of data on weather and 4 others on the 2 panels' outputs. Virtual panels performance data for the new MATLAB® based model was derived from the real weather data so that 4 additional pieces of data were added to each of the above sets. Thus, 34398 data pieces were available for reconfiguration and comparison with TRNSYS simulation results for the two panels.

From the resulting information, the following key performance indicators and ratios were deduced:

- The new tracking device improved daily electrical energy yields by variable ratios over the period ranging from 1.05 to 1.84. In total however, a 34% gain over the fixed panel yield was obtained for the entire period.
- On about 50% of the days, the new tracking device was slightly inaccurate owing to wind disturbances.
- The new MATLAB® model correlated better with experimental data when compared with the TRNSYS's model by factors of 1.11 and 1.28 for a fixed and a tracking panel respectively.

Considering that this tracker was designed for domestic use in sub-Sahara Africa, the results seem to suggest that it would be most appropriate in the southern mid tropical areas where according to [15] – [17], skies are most clear and wind speeds are low. In the great lakes subregion - with convectional rainfall in mid afternoons - chances are that it would also be valuable since most of its energy gains are made in mid morning and late afternoons. At this stage however, it is not clear how useful the tracker would be in the windy and dusty Sahel subregion of west and mid northern Africa. This tracker would perhaps be least useful in the equatorial rain forests of Congo river basin. All said, further experimentation in the said subregions would be most appropriate before adoption on a mass scale.

References

[1] K. E. Kanyarusoke, J. Gryzagoridis and G. Oliver, "Are solar tracking technologies feasible for domestic applications in rural tropical Africa?" *JESA*, vol. *26*, no. *1*, pp. 86-95, 2015.

[2] K. E. Kanyarusoke and J. Gryzagoridis, "A hydraulic mechanism. Solar Tracker," South Africa Patent application P72557Z - 2015/09278P00, Dec, 21, 2015.

[3] M. J. Clifford and D. Eastwood. (July, 2004). Design of a novel passive solar tracker. Solar Energy. [Online]. 77, pp. 269–280. Available: http://ac.els-cdn.com/S0038092X04001483/1-s2.0-S0038092X04001483-main.pdf?_tid=62b42852-c9a4-11e5-bcc5-00000aab0f26&acdnat=1454414537_c97ff18104b23154870a11e6a4969981

[4] F. J. G. Gil, M. D. Martín, J. P. Vara and J. R. Calvo, "A review of solar tracker patents in Spain," in *Proc.3rd WSEAS Int. Conf. on Renewable energy sources*, Spain, 2009, pp. 292-297.

[5] B-J. Huang, Y-C. Huang, G-Y. Chen, P-c. Hsu and K. Li. "Improving solar PV system efficiency using one-axis 3-position sun tracking," *Energy Procedia,* vol. 33, pp. 280-287, 2013.

[6] S.Bazyari, R. Keypour, S. Farhangi, A. Ghaedi and K. Bazyari. "A study on the effects of solar tracking systems on the performance of photovoltaic power plants," *JPEE,* vol. 2, pp. 718 -728, 2014.

[7] J. R. B. del Rosario, R. C. Gustilo and E. P. Dadios, "Optimisation of a small scale dual-axis solar tracking system using nanowatt technology," *JOACE,* vol. 2 no.2, pp. 134-137, 2014.

[8] J. A. Duffie and W. A. Beckman, *Solar Engineering of Thermal Processes*. 4th ed. Solar Energy Laboratory, University of Wisconsin-Madison, USA, Wiley, 2013, pp. 91-97.

[9] R. Perez, P. Ineichen, S. J. Michalsky and R. Stewart, "Modelling daylight availability and irradiance components from direct and global irradiance," *Solar Energy*, vol. 44 no.5, pp. 271-289, 1990.

[10] G. N. Tiwari, *Solar Energy: Fundamentals, Design, Modelling and Applications,* New Delhi India, Narosa, 2002 pp.16-40.

[11] S. A. Kalogirou, *Solar Energy Engineering Processes and Systems*. 2nd ed. Oxford, UK, Elsevier Inc., 2014, pp.51-106.

[12] S. A. Klein, J. A. Duffie, J. C. Mitchell, J. P. Kummer, J. W. Thornton, E. Bradley, D. A. Arias, W. A. Beckman, N. A. Duffie, J. E. Braun, *et al. TRNSYS 17 A transient system simulation program.* Madison, USA: Solar Energy Laboratory, University of Wisconsin, 2012.

[13] K. E. Kanyarusoke, J. Gryzagoridis and G. Oliver, "Predicting photovoltaic panel yields in sub-Sahara Africa," in *Proc. ICEAS,* Beijing, China, 2012, pp. 223-255.

[14] D. L. King, W. E. Boyson and J. A, Kratochvill, (2004, Dec.). Photovoltaic Array Performance Model. SANDIA Report SAND2004-3535, Sandia National Laboratories, Albuquerque, New Mexico.[Online] Available: http://prod.sandia.gov/techlib/access-control.cgi/2004/043535.pdf

[15] A. Hoscilo, H. Balzter, E. Bartholomé, M. Boschetti, P. A. Brivio, A. Brink and M. Clerici, (2015). A conceptual model for assessing rainfall and vegetation trends in sub-Saharan Africa from satellite data. *Int. Journal of Climatology* [on line], 35, pp. 3582-3592 Available: Onlinelibrary.wiley.com/doi/10.1002/joc.4231/epdf

[16] M. Haile, (2005). Weather patterns, food security and humanitarian response in sub-Saharan Africa. *Philosophical Transactions of The Royal Society B: Biological Sciences*, 360(1463), 2169 - 2182. http://doi.org/10.1098/rstb.2005.1746.

[17] L. Guertin, (nd). *Earth 105: Environments of Africa – Geology and climate history.* Penn. State College of Earth and Mineral Sciences, [Online]. Available: http://courseware.e-education.psu.edu/courses/earth105new/content/home.html

Authors Bios and Photographs

Kant E. Kanyarusoke received his 1st class honours BSc. Eng. degree from Makerere University, Uganda in 1982, a MSc. (Mech. Eng.) from University of Lagos, Nigeria in 1985 and a cum laude PG HDHET from CPUT in 2009. He is now a doctoral candidate in Mechanical Engineering at CPUT. A member of ASHRAE, he has about 20 years industrial experience in Chemicals, Foods and Beverages factories and in small scale industrial setups in several sub-Sahara African countries. He has an almost equal number of years in university teaching and engineering education. He now lectures Machine Design and Thermodynamics and supervises PG solar engineering students at CPUT.

Jasson Gryzagoridis Pr. Eng. BSc, MSc, PhD is a registered professional engineer, and holds degrees from Lamar University, Texas A&M University and the University of Cape Town respectively. He is an Adjunct Professor acting as post graduate student's mentor at the Mech. Eng. Department at Cape Peninsula University of Technology (CPUT).

Presenting author: The paper will be presented by Kant E. Kanyarusoke